Disease Markers 27 (2009) 239–252
DOI 10.3233/DMA-2009-0670
IOS Press

Molecular network analysis suggests aberrant CREB-mediated gene regulation in the Alzheimer disease hippocampus

Jun-ichi Satoh[a,*], Hiroko Tabunoki[a] and Kunimasa Arima[b]
[a]*Department of Bioinformatics and Molecular Neuropathology, Meiji Pharmaceutical University, 2-522-1 Noshio, Kiyose, Tokyo 204-8588, Japan*
[b]*Department of Psychiatry, National Center Hospital, National Center of Neurology and Psychiatry, 4-1-1 Ogawahigashi, Kodaira, Tokyo 187-8551, Japan*

Abstract. The pathogenesis of Alzheimer disease (AD) involves the complex interaction between genetic and environmental factors affecting multiple cellular pathways. Recent advances in systems biology provide a system-level understanding of AD by elucidating the genome-wide molecular interactions. By using KeyMolnet, a bioinformatics tool for analyzing molecular interactions on the curated knowledgebase, we characterized molecular network of 2,883 all stages of AD-related genes (ADGs) and 559 incipient AD-related genes (IADGs) identified by global gene expression profiling of the hippocampal CA1 region of AD brains in terms of significant clinical and pathological correlations (Blalock et al., Proc Natl Acad Sci USA 101: 2173-2178, 2004). By the common upstream search, KeyMolnet identified cAMP-response element-binding protein (CREB) as the principal transcription factor exhibiting the most significant relevance to molecular networks of both ADGs and IADGs. The CREB-regulated transcriptional network included upregulated and downregulated sets of ADGs and IADGs, suggesting an involvement of generalized deregulation of the CREB signaling pathway in the pathophysiology of AD, beginning at the early stage of the disease. To verify the *in silico* observations *in vivo*, we conducted immunohistochemical studies of 11 AD and 13 age-matched control brains by using anti-phoshorylated CREB (pCREB) antibody. An abnormal accumulation of pCREB imunoreactivity was identified in granules of granulovacuolar degeneration (GVD) in the hippocampal neurons of AD brains. These observations suggest that aberrant CREB-mediated gene regulation serves as a molecular biomarker of AD-related pathological processes, and support the hypothesis that sequestration of pCREB in GVD granules is in part responsible for deregulation of CREB-mediated gene expression in AD hippocampus.

Keywords: Alzheimer disease, CREB, granulovacuolar degeneration, keymolnet, molecular network, systems biology

1. Introduction

Alzheimer disease (AD) is the most common cause of dementia worldwide, affecting the elderly population, characterized by the hallmark pathology of amyloid-β (Aβ) deposition and neurofibrillary tangle (NFT) formation in the brain. The complex interaction between genetic and environmental factors affecting multiple cellular pathways plays a role in the pathogenesis of AD [1]. The completion of the Human Genome Project in 2003 allows us to systematically characterize the comprehensive disease-associated profiles of the whole human genome. It promotes us to identify disease-specific and stage-specific molecular signatures and biomarkers for diagnosis and prediction of prognosis, and druggable targets for therapy [2]. Actually, global transcriptome analysis of AD brains identified a battery of genes aberrantly regulated in AD, whose role has not been previously

*Corresponding author: Prof. Dr. Jun-ichi Satoh, Department of Bioinformatics and Molecular Neuropathology, Meiji Pharmaceutical University, 2-522-1 Noshio, Kiyose, Tokyo 204-8588, Japan. Tel./Fax: +81 42 495 8678; E-mail: satoj@my-pharm.ac.jp.

ISSN 0278-0240/09/$17.00

predicted in its pathogenesis. They include reduced expression of kinases/phosphatases, cytoskeletal proteins, synaptic proteins, and neurotransmitter receptors in NFT-bearing CA1 neurons [3], downregulaton of neurotrophic factors and upregulation of proapoptotic molecules in the hippocampal CA1 region [4], disturbed sphingolipid metabolism in various brain regions during progression of AD [5], and overexpression of the AMPA receptor GluR2 subunit in synaptosomes of prefrontal cortex [6]. However, in global expression analysis, the important biological implications are often left behind to be characterized, because the huge amount of high-density microarray data is highly complex. Furthermore, cardinal observations obtained from *in silico* data analysis should be validated by independent wet lab experiments.

Recent advances in systems biology enable us to illustrate a cell-wide map of the complex molecular interactions with aid of the literature-based knowledgebase of molecular pathways [7,8]. In the scale-free molecular network, targeted disruption of several critical components, on which the biologically important molecular connections concentrate, could disturb the whole cellular function by destabilizing the network [9]. Thus, molecular network analysis goes beyond gene-by-gene analysis to shed light on a system-level understanding of molecular relationships among individual genes and networks.

The present study is designed to conduct molecular network analysis of a published microarray dataset of Blalock et al. [10]. It contains genome-wide expression profiling of hippocampal CA1 tissues derived from 22 AD patients with well-defined clinical and pathological stages. They identified 3,413 all stages of AD-related genes (ADGs) and 609 incipient AD-related genes (IADGs), and characterized overrepresented genes by using a bioinformatics tool named Expression Analysis Systematic Explorer (EASE). They found upregulation of tumor suppressors, oligodendrocyte growth factors, and protein kinase A (PKA) modulators, along with downregulation of protein folding/metabolism/transport machinery molecules in incipient AD (IAD) [10]. Recently, a different study followed up analysis of this dataset by weighted gene coexpression network analysis (WGCNA) that calculates a matrix containing all pairwise Pearson correlations between whole microarray probe sets across all subjects in an unsupervised manner. They identified AD-related coexpression modules that play key roles in synaptic transmission, extracellular transport, mitochondrial and metabolic functions, and myelination [11]. However, all of these studies did not clarify the common upstream transcription factors governing molecular networks, closely associated with deregulated gene expression in AD brains. By using KeyMolnet, a bioinformatics tool for analyzing molecular interactions on the curated knowledgebase [12], we characterized the most relevant molecular network of AD brain transcriptome, composed of the genes coordinately regulated by putative common upstream transcription factors.

2. Materials and methods

2.1. The dataset

We performed molecular network analysis of ADGs and IADGs, derived from a dataset of Blalock et al. [10]. It contains gene expression profiling of frozen tissues of the CA1 hippocampus, performed by analyzing with the Affymetrix Human Genome HG-U133A chip that contains 22,215 transcripts. The complete dataset is available from Gene Expression Omnibus (GEO) database (GSE1297). RNA was isolated from the samples of 31 age-matched individuals, composed of nine control subjects, seven patients with incipient AD (IAD), eight with moderate AD, and seven with severe AD [10]. The dataset was normalized following the Microarray Analysis Suite 5.0 (MAS5) algorithm. The clinical stage of AD was defined by the Mini-Mental State Examination (MMSE) score, i.e. control (MMSE $>$ 25), incipient AD (MMSE 20–26), moderate AD (MMSE 14–19), and severe AD (MMSE $<$ 14). The neurofibrillary tangle (NFT) burden was determined in each brain sample, which always showed an inverse relationship with the MMSE score. The statistical correlation between the expression levels of individual genes and the MMSE and NFT scores was evaluated by Pearson's correlation tests and ANOVA. With respect to overall correlations across 31 subjects, the study identified 3,413 ADGs, composed of 1,977 upregulated and 1,436 downregulated genes in all stages of AD patients versus control subjects. The study also identified 609 IADGs, composed of 431 upregulated and 178 downregulated genes in IAD patients versus control subjects.

2.2. Gene ID conversion

We converted Affymetrix probe IDs into the corresponding National Center for Biotechnology Information (NCBI) Entrez Gene IDs by using the

Database for Annotation, Visualization and Integrated Discovery (DAVID) 2008 Gene ID conversion tool (david.abcc.ncifcrf.gov) [13]. Then, we excluded a set of non-annotated genes, overlapping genes, and those listed concurrently in both upregulated and downregulated classes.

2.3. Molecular network analysis

KeyMolnet is a comprehensive knowledgebase, originally developed by the Institute of Medicinal Molecular Design (IMMD), Tokyo, Japan [12]. It covers virtually all the relationships heretofore reported among human genes, molecules, diseases, pathways and drugs, whose information is manually collected, carefully curated, and regularly updated by expert biologists. The database is categorized into the core contents collected from selected review articles with the highest reliability, or the secondary contents extracted from abstracts of PubMed database and Human Protein Reference database (HPRD). By importing microarray data, such as the list of Entrez Gene ID and fold changes of individual probes, KeyMolnet automatically provides corresponding molecules as a node on networks.

The common upstream search is a mode of network analysis that extracts the most relevant molecular network composed of the genes coordinately regulated by putative common upstream transcription factors. The generated network was compared side by side with 403 human canonical pathways of the KeyMolnet library. To reduce the potential bias toward the selection of major pathways, all well-established biological pathways covering both major and minor classes were collected by extensive search of valid review articles with journal impact factors greater than 10. Further information on the canonical pathways of KeyMolnet is available from IMMD upon request (www.immd.co.jp/en/keymolnet/index.html). The algorithm counting the number of overlapping molecular relations between the extracted network and the canonical pathway makes it possible to identify the canonical pathway showing the most significant contribution to the extracted network. It is constructed by modification of the algorithm developed for GO::TermFinder [14]. The significance in the similarity between the extracted network and the canonical pathway is scored following the formula, where O = the number of overlapping molecular relations between the extracted network and the canonical pathway, V = the number of molecular relations located in the extracted network, C = the number of molecular relations located in the canonical pathway, T = the number of total molecular relations composed of approximately 110,000 sets, and the X = the sigma variable that defines coincidence.

$$\text{Score} = -\log_2(\text{Score}(p))$$

$$\text{Score}(p) = \sum_{x=O}^{Min(C,V)} f(x)$$

$$f(x) = {}_C C_x \cdot {}_{T-C} C_{V-x} / {}_T C_V$$

2.4. Immunohistochemistry

The autopsied brain samples were provided by Research Resource Network (RRN), Japan. Written informed consent was obtained form all the cases. The Ethics Committee of National Center of Neurology and Psychiatry approved the present study. The study population consists of 11 AD patients composed of five men and six women with the mean age of 71 ± 9 years, and 13 other neurological disease (termed as non-AD) patients composed of six men and seven women with the mean age of 69 ± 9 years. The non-AD cases include three patients with Parkinson disease (PD), two with multiple system atrophy (MSA), four with amyotrophic lateral sclerosis (ALS), and four with myotonic dystrophy. The average of brain weight was 1,038 ± 163 gram in AD cases and 1,195 ± 182 gram in non-AD cases. Brain tissues of the hippocampus and the motor cortex were fixed with 4% paraformaldehyde (PFA), embedded in paraffin, and processed for ten micron-thick serial sections. All AD cases were satisfied with the Consortium to Establish a Registry for Alzheimer's Disease (CERAD) criteria for diagnosis of definite AD [15]. They were categorized into the stage C of amyloid deposition and the stage VI of neurofibrillary degeneration, following the Braak's staging [16].

The immunohistochemistry protocol was described elsewhere [17]. In brief, after deparaffination, tissue sections were heated in 10 mM citrate sodium buffer, pH 6.0 by autoclave at 125°C for 30 sec in a temperature-controlled pressure chamber (Dako, Tokyo, Japan). They were incubated with 3% hydrogen peroxide-containing methanol to block the endogenous peroxidase activity, and with phosphate-buffered saline (PBS) containing 10% normal goat serum (NGS) at room temperature (RT) for 15 min to block non-specific staining. Then, tissue sections were stained at 4°C overnight with rabbit polyclonal anti-phoshorylated cAMP-response element-binding protein (pCREB) an-

tibody at a dilution of 1:1,000 (Y011052; Applied Biological Materials, Richmond, BC, Canada). This antibody was produced against a synthesized phosphopeptide spanning R-P-SP-Y-R, derived from the human CREB1 amino acid sequences surrounding the serine 133 residue (Ser-133), and purified by affinity-chromatography with an epitope-specific phosphopeptide. The specificity of the antibody was verified by western blot analysis of a human neuronal cell line exposed to forskolin in culture (not shown). After several washes, the tissue sections were incubated with horseradish peroxidase (HRP)-conjugated anti-rabbit antibody (Nichirei, Tokyo, Japan), and colorized with DAB substrate (Vector Laboratories, Burlingame, CA, USA), followed by a counterstain with hematoxylin. The adjacent sections were immunolabeled with mouse monoclonal anti-GFAP antibody (Nichirei). For negative controls, the step of incubation with primary antibodies was omitted.

3. Results

3.1. Transcriptome dataset of Alzheimer disease hippocampus

The dataset of Blalock et al. [10] contains genome-wide transcriptome of the hippocampus CA1 region, derived from nine control subjects, seven patients with incipient AD (IAD), eight with moderate AD, and seven with severe AD. They identified 3,413 all stages of AD-related genes (ADGs) and 609 IAD-related genes (IADGs) based on significant clinical and pathological correlations. We performed extensive curation of their data, and extracted 2,883 Entrez Gene IDs of ADGs, composed of 1,675 upregulated and 1,208 downregulated genes in all stages of AD patients versus control subjects (Supplementary Tables 1 and 2 online). We also identified 559 Entrez Gene IDs of IADGs, composed of 395 upregulated and 164 downregulated genes in IAD patients versus control subjects (Supplementary Tables 3 and 4 online).

3.2. The molecular network analysis of ADGs and IADGs identified CREB as a central transcription factor

First, we imported 2,883 Entrez Gene IDs of ADGs, along with the expression levels, into KeyMolnet (the version 4.9.9.616 of July 1, 2009). The common upstream search of the core contents generated a complex network composed of 508 fundamental nodes with 735 molecular relations, arranged with respect to subcellular location of the molecules by the editing function of KeyMolnet (Fig. 1). By statistical evaluation, the extracted network showed the most significant relationship with transcriptional regulation by CREB with the score of 229 and score (p) = 1.141E-069, where CREB is located as a common upstream transcription factor that has direct connections with 50 nodes, all of which are known CRE-responsive genes (Fig. 2 and Table 1). Unexpectedly, the CREB-regulated transcriptional network is comprised of not only 17 upregulated ADGs but also 26 downregulated ADGs. These results suggest not simply either overactivation or hypoactivation of CREB but an involvement of generalized deregulation of the CREB signaling pathway in the pathophysiology of AD. The second rank pathway was transcriptional regulation by nuclear factor kappa B (NF-κB) with the score of 158 and score (p) = 1.945E-048 (Supplementary Fig. 1 online), while the third rank was transcriptional regulation by vitamin D receptor (VDR) with the score of 140 and score (p) = 5.841E-042 (Supplementary Fig. 2 online).

Next, we imported 559 Entrez Gene IDs of IADGs and the expression levels into KeyMolnet. Subsequently, the common upstream search of the core contents generated a less complex network composed of 143 fundamental nodes with 190 molecular relations (Fig. 3). By statistical evaluation, the extracted network showed again the most significant relationship with transcriptional regulation by CREB with the score of 71 and score (p) = 3.325E-022, comprised of 5 upregulated and 5 downregulated IADGs (Fig. 4 and Table 1). These results suggest that functional impairment of CREB in the AD hippocampus is beginning at the early stage of the disease. The second rank pathway was transcriptional regulation by NF-κB or by glucocorticoid receptor (GR) with the identical score of 53 and score (p) = 1.163E-016 between both.

3.3. Granulovacuolar degeneration in hippocampal neurons of AD brains expressed pCREB immunoreactivity

It is well known that a wide range of extracellular stimuli activates CREB by inducing phosphorylation of Ser-133 on CREB, thereby it functions as a transcriptional activator [18,19]. Because the molecular network of both ADGs and IADGs reflects persistent impairment of CREB function in the AD hippocampus, we studied the expression of Ser-133-phosphorylated

Table 1
The list of 51 genes constructing the CREB-regulated transcriptional network in AD hippocampus

KeyMolnet symbol	Gene name	Upregulation or downregulation[a]	Involvement in IAD network	Swiss-Prot ID
14-3-3epsilon	14-3-3 protein epsilon	down		P62258
AChE	acetylcholinestrase	down		P22303
AhR	arylhydrocarbon receptor	km		P35869
BCKDH	branched-chain alpha-keto acid dehydrogenase	down		P09622, P11182, P12694, P21953
Bcl-2	B-cell lymphoma 2	up		P10415
BiP	78 kDa glucose-regulated protein	down	yes	P11021
BRCA1	breast cancer type 1 susceptibility protein	up		P38398
C/EBPb	CCAAT/enhancer binding protein beta	km	yes	P17676
CCK	cholecystokinin	down		P06307
CDK5	cyclin dependent kinase 5	down		Q00535
ChromograninA	chromogranin A	down		P10645
CPT	carnitine palmitoyl transferase	up	yes	P50416, Q92523, Q8TCG5, P23786
CREB	cAMP-response-element-binding-protein	km	yes	P16220
CRF	corticotropin-releasing factor	down	yes	P06850
cyclinA	cyclin A	down		P78396, P20248
cyto-c	cytochrome c	down		P99999
DIO2	type II iodothyronine deiodinase	down		Q92813
Egr1	early growth response protein 1	up		P18146
ENO2	neuron-specific enolase	down		P09104
FN1	fibronectin 1	down		P02751
GADD34	protein phosphatase 1, regulatory subunit 15A	up		O75807
GluR1	glutamate receptor 1	down		P42261
GR	glucocorticoid receptor	km	yes	P04150
GS	glutamine synthetase	down	yes	P15104
HO-1	heme oxygenase 1	up		P09601
ICAM-1	intercellular adhesion molecule 1	up		P05362
IGF1	insulin-like growth factor 1	down		P01343, P05019
IL-6	interleukin-6	up		P05231
JunD	transcription factor Jun-D	up	yes	P17535
LDH	L-lactate dehydrogenase	down		Q6ZMR3, Q9BYZ2, P00338, P07195, P07864
MITF	microphthalmia-associated transcription factor	up	yes	O75030
MnSOD	manganese superoxide dismutase	up		P04179
NF-L	neurofilament triplet L protein	down		P07196
NPY	neuropeptide Y	down		P01303
NR4A2	orphan nuclear receptor NR4A2	km		P43354
ODC	ornithine decarboxylase	up		P11926
PC	prohormone convertase	down		P29120, P16519, Q16549
PCB	pyruvate carboxylase	up	yes	P11498
PCNA	proliferating cell nuclear antigen	down		P12004
PER1	period circadian protein 1	up	yes	O15534
PER2	period circadian protein 2	up		O15055
Pit-1	pituitary-specific positive transcription factor 1	km	yes	P28069
PPT-A	preprotachykinin A	down	yes	P20366
proenkeph	proenkephalin	down		P01213, P01210
SGK	serum- and glucocorticoid-inducible kinase	up	yes	O00141, Q9HBY8, Q96BR1
SST	somatostatin	down	yes	P61278
STAT3	signal transducer and activator of transcription 3	km	yes	P40763
SynapsinI	synapsin-1	down		P17600
TGFb2	transforming growth factor beta 2	up		P61812
TyrAT	tyrosine aminotransferase	up		P17735
VIP	vasoactive intestinal peptide	down		P01282

Km represents additional nodes unlisted in the original set of 2,883 ADGs but automatically incorporated from KeyMolnet core contents following the network-searching algorithm.

CREB (pCREB) in 11 AD and 13 age-matched control brains by immunohistochemistry. The granular components of granulovacuolar degeneration (GVD), accumulated in the cytoplasm of hippocampal pyramidal neurons in both AD and non-AD brains, expressed strong immunoreactivity against pCREB (Fig. 5, panels a-d). However, the nuclei of hippocampal pyramidal neurons were devoid of pCREB immunoreac-

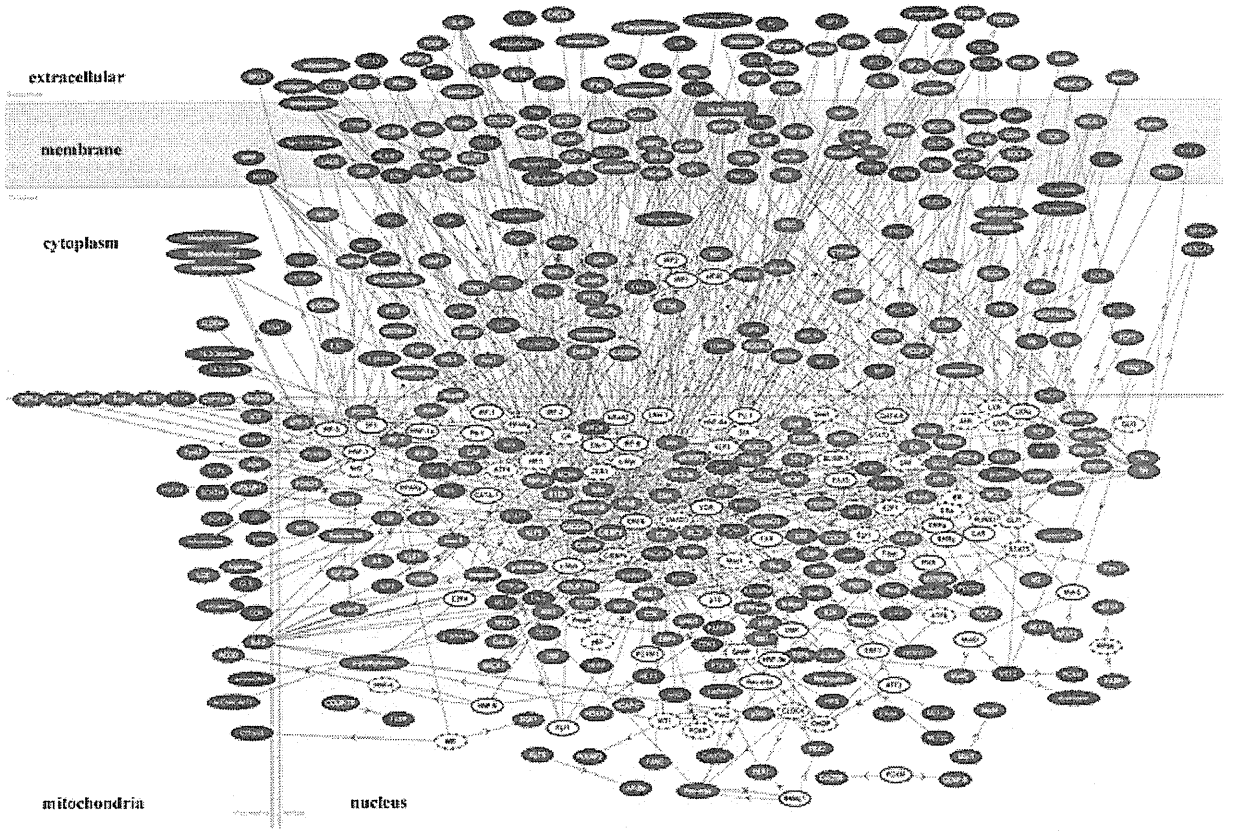

Fig. 1. Molecular network of all stages of AD-related genes (ADGs). The list of 2,883 Entrez Gene IDs corresponding to ADGs was imported into KeyMolnet. The common upstream search of the core contents generated a network composed of 508 fundamental nodes with 735 molecular relations, arranged with respect to subcellular location of the molecules. Red nodes represent upregulated genes, whereas blue nodes represent downregulated genes. White nodes exhibit additional nodes extracted automatically from the core contents incorporated in the network to establish molecular connections. The direction of molecular relation is indicated by red-colored dash line with arrow (transcriptional activation) or blue-colored dash line with arrow and stop (transcriptional repression).

tivity. In addition, the vacuolar component of GVD lacked pCREB immunoreactivity, while neuritic processes of hippocampal neurons expressed variable levels of pCREB immunoreactivity (Fig. 5, panel c). pCREB-immunoreactive GVD-bearing neurons were distributed chiefly in the CA1-CA3 sectors. Senile plaques and neurofibrillary tangles were completely devoid of pCREB immunolabeling. Although the number of pCREB-immunoreactive GVD-bearing neurons was varied among the cases, it was significantly greater in the hippocampus of AD compared with non-AD ($p = 0.00020$ by Mann-Whiteney's U test) (Fig. 6). pCREB-immunoreactive GVD-bearing neurons were occasionally found in the CA4 and subicular regions of AD brains, but barely detectable in the corresponding regions of non-AD brains. In both AD and non-AD brains, substantial numbers of neuronal axons distributed in the white matter of the motor cortex expressed intense pCREB immunoreactivity (Fig. 5, panel e). In both AD and non-AD brains, a subpopulation of reactive astrocytes and almost all ependymal cells expressed strong pCREB immunoreactivity, but it was located predominantly in their nuclei (Fig. 5, panel f). In both AD and non-AD brains, most neurons except for hippocampal pyramidal neurons did not express discernible pCREB immunoreactivity in their cell bodies and nuclei. Neither oligodendrocytes nor microglia expressed pCREB immunoreactivity in any cases examined.

4. Discussion

Since microarray analysis usually produces a large amount of gene expression data at one time, it is often difficult to find out the meaningful relationship be-

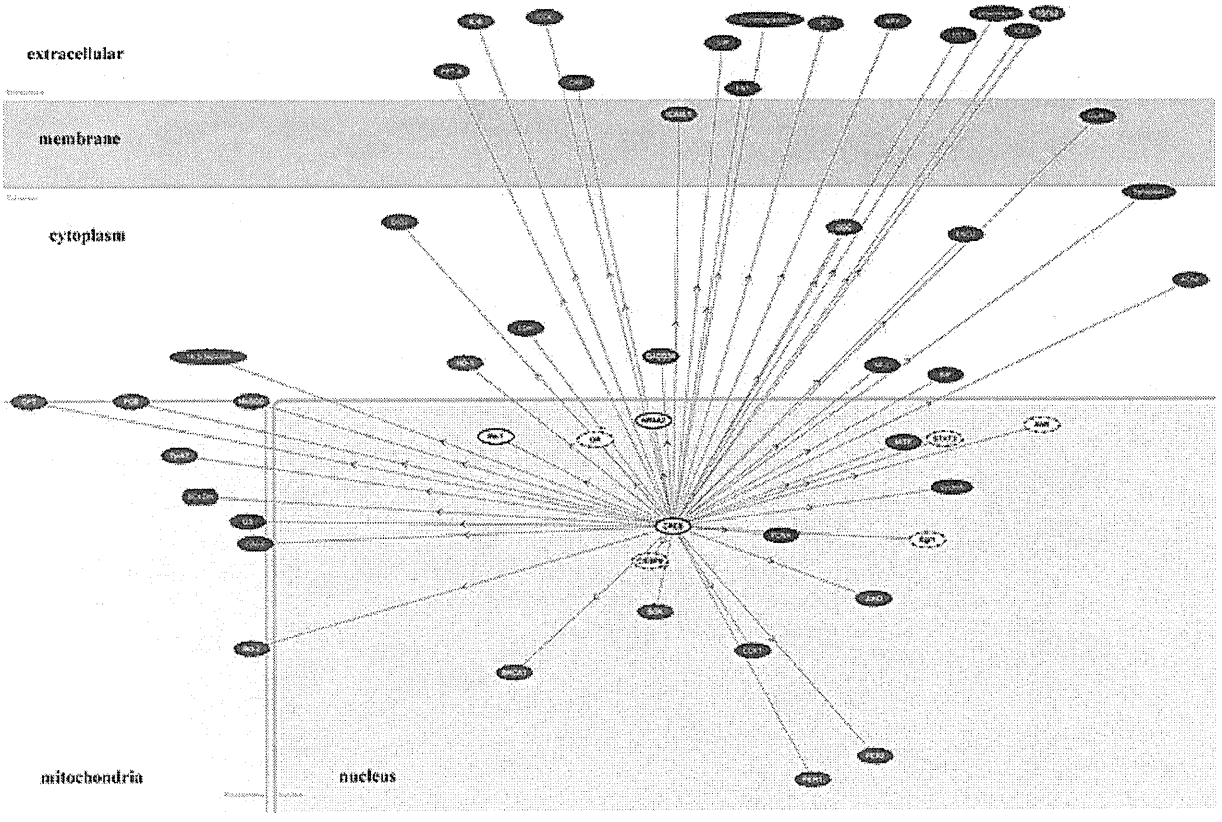

Fig. 2. The CREB-regulated transcriptional network of ADGs. The CREB-regulated transcriptional network extracted from the ADG network of Fig. 1 consists of a central node of CREB and 50 connecting nodes of CREB target genes listed in Table 1.

tween gene expression profile and biological implications from such a large quantity of available data. To overcome this difficulty, we have made a breakthrough to identify the molecular network most closely associated with microarray data by using a novel bioinformatics tool named KeyMolnet [12]. KeyMolnet includes the highly reliable information on a wide range of human proteins, small molecules, molecular relations, diseases, and drugs. All the contents are manually collected and carefully curated by experts from the literature and public databases. The application of KeyMolnet has an advantage that the user can easily merge microarray data with the comprehensive knowledgebase to characterize pathophysiologically meaningful networks from the high-throughput gene expression data [20,21]. In particular, the common upstream search is the most powerful approach to identify a battery of common transcription factors governing molecular networks closely associated with aberrant gene expression. By using KeyMolnet, we characterized the molecular network of 2,883 ADGs and 559 IADGs that show significant correlations with MMSE score and NFT burden in either all stages of AD or the early stage of AD [10]. We identified CREB as the central transcription factor that exhibits the most significant relevance to molecular networks of both ADGs and IADGs.

CREB is the prototype stimulus-inducible transcription factor binding as a dimer to a conserved cAMP-responsive element (CRE) of the target genes [18,19]. CREB is promptly activated in response to a wide range of extracellular stimuli, such as growth factors, peptide hormones, and neuronal activity, all of which activate various protein kinases such as PKA, mitogen-activated protein kinases (MAPKs), and Ca^{2+}/calmodulin-dependent protein kinases (CAMKs). They phosphorylate Ser-133 located in the KID domain of CREB. The phosphorylation of Ser-133 on CREB (pCREB) induces the recruitment of a transcriptional coactivator named CREB binding protein (CBP), thereby activates the expression of CRE-responsive genes. The CREB target genes play key roles in neuronal devel-

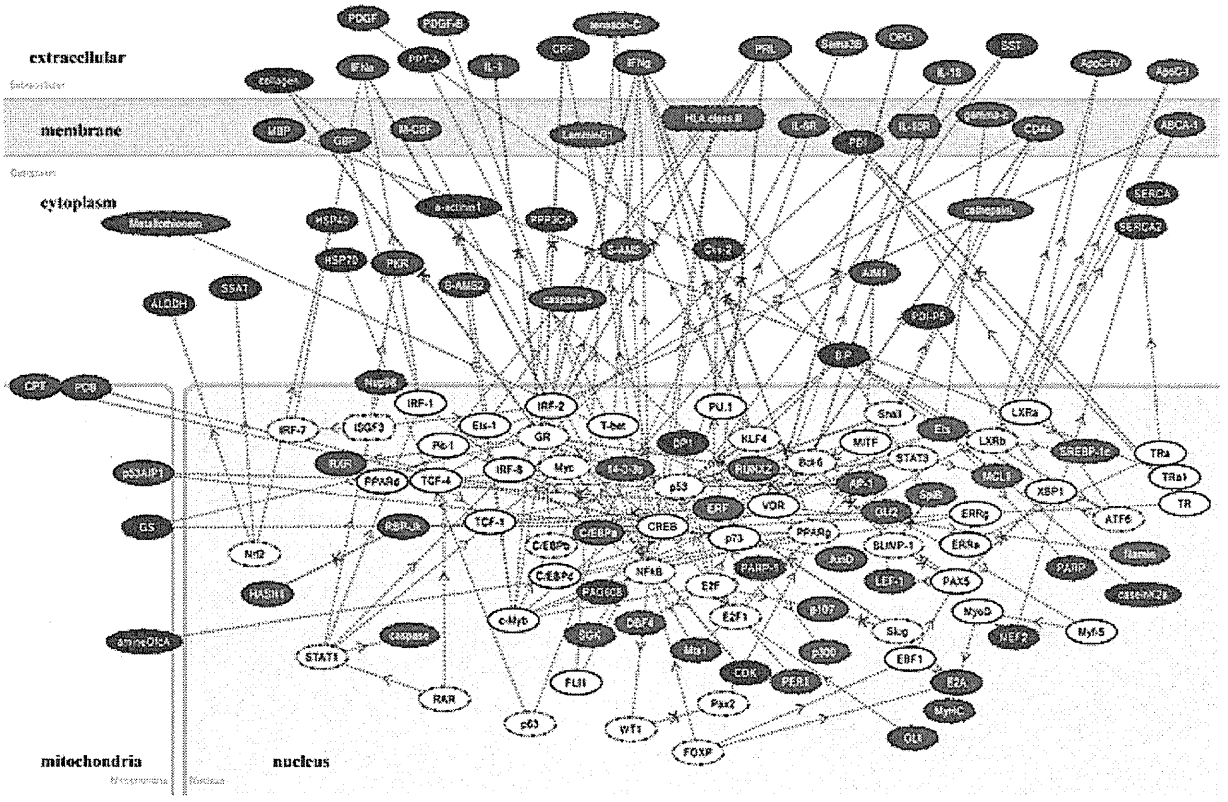

Fig. 3. Molecular network of incipient AD-related genes (IADGs). The list of 559 Entrez Gene IDs corresponding to IADGs was imported into KeyMolnet. The common upstream search of the core contents generated a network composed of 143 fundamental nodes with 190 molecular relations, arranged with respect to subcellular location of the molecules. Red nodes represent upregulated genes, whereas blue nodes represent downregulated genes. White nodes exhibit additional nodes extracted automatically from the core contents incorporated in the network to establish molecular connections. The direction of molecular relation is indicated by red-colored dash line with arrow (transcriptional activation) or blue-colored dash line with arrow and stop (transcriptional repression).

opment, synaptic plasticity, and neuroprotection in the central nervous system (CNS). Currently, we are able to search thousands of CREB target genes via the web-accessible database (natural.salk.edu/CREB) [22]. In the present study, the CREB-regulated transcriptional network consisted of both upregulated and downregulated sets of ADGs and IADGs. These observations suggest not simply either overactivation or hypoactivation of CREB but an involvement of generalized deregulation of the CREB signaling pathway in the pathophysiology of AD, emerging at the early stage of the disease.

To verify the *in silico* observations *in vivo*, we conducted immunohistochemical studies of 11 AD and 13 age-matched non-AD control brains by using anti-pCREB antibody. We identified aberrant pCREB immunoreactivity concentrated in granules of GVD in the hippocampus of both AD and non-AD brains, where the number of pCREB-immunoreactive GVD-bearing neurons was significantly greater in AD than non-AD cases. These results suggest that pCREB-immunoreactive GVD does not itself serve as an AD-specific diagnostic marker. However, these observations would support the hypothesis that sequestration of pCREB in GVD granules might be in part attributable to disturbed CREB-regulated gene expression in AD hippocampus.

Physiologically, CREB plays a pivotal role in the long-term memory formation in CA1 hippocampal neurons [23]. A previous study by western blot analysis showed that pCREB levels are reduced in AD brain tissues, although the cellular and subcellular location of pCREB was not characterized [24]. In a rat model, cortical impact injury induces a cognitive impairment, associated with reduced expression of CREB and target genes in the ipsilateral hippocampus [25]. A phosphodiesterase-4 inhibitor rolipram, by activating the cAMP/PKA/CREB signaling pathway, ameliorates deficits in long-term potential and cognitive function

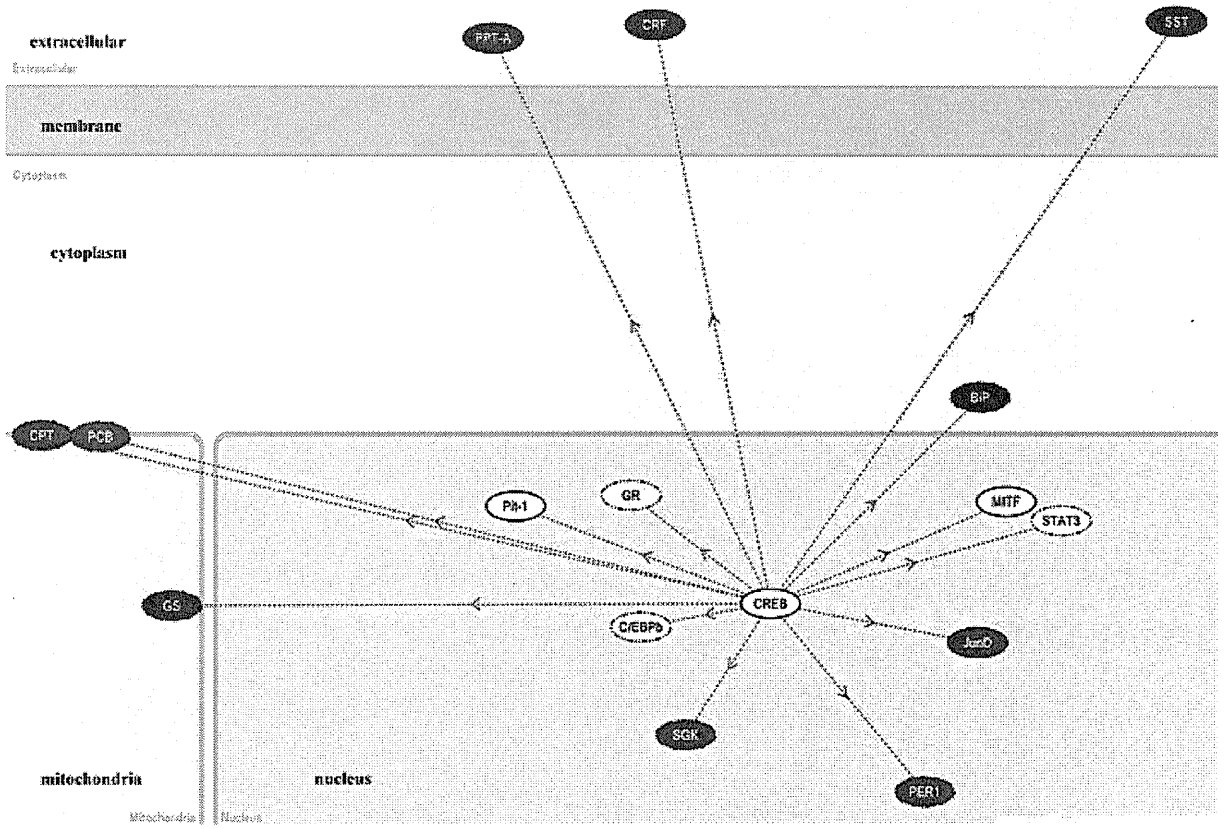

Fig. 4. The CREB-regulated transcriptional network of IADGs. The CREB-regulated transcriptional network extracted from the IADG network of Fig. 3 consists of a central node of CREB and 15 connecting nodes of CREB target genes listed in Table 1.

in a transgenic mouse model of AD [26]. Overactivation of calpain induces proteolysis of PKA subunits, resulting in inactivation of CREB in AD brains [27]. High levels of intracellular Aβ induce sustained hyperphosphorylation of CREB that blocks nuclear translocation of pCREB, resulting in inactivation of CREB-regulated gene expression [28]. The Aβ oligomers inactivate MAPKs, PKA, and cyclic GMP-dependent protein kinase essential for CREB activation in hippocampal neurons [29–31]. Long-term treatment with green tea catechin reduces the levels of Aβ oligomers, thereby restores the expression of CREB target genes, such as BDNF and PSD95, in the hippocampus [32]. All of these observations support a possible scenario that a defect in the CREB-mediated signaling pathway in hippocampal neurons causes cognitive disturbance during progression of AD. Therefore, CREB serves as a promising molecular target for treatment of dementia in AD [33].

The accumulation of misfolded cellular proteins within neurons, due to a defect in the clearance system, such as the ubiquitin-proteasome system (UPS) and the autophagic-lysosomal system, is a pathological hallmark of various neurodegenerative diseases [34]. Degradation of CREB involves nuclear export of CREB, modification by polyubiquitination, and processing for proteasomes, suggesting that UPS is a major system for CREB degradation under normal physiological conditions [35,36]. We identified an abnormal accumulation of pCREB in GVD granules of hippocampal neurons in AD brains. GVD is a pathological change characterized by electron-dense granules within double membrane-bound cytoplasmic vacuoles that highly resemble autophagosomes [37]. The emergence of GVD is confined to hippocampal pyramidal neurons of AD brains, and infrequently found in those of other neurodegenerative diseases. GVD is barely detectable in other brain regions. It plays a role in sequestration and degradation of unnecessary proteins and organelles in neurons exposed to aging-related stressful insults [37]. The active forms of caspase-3, glycogen synthase kinase-3β (GSK-3β), c-Jun N-terminal kinase

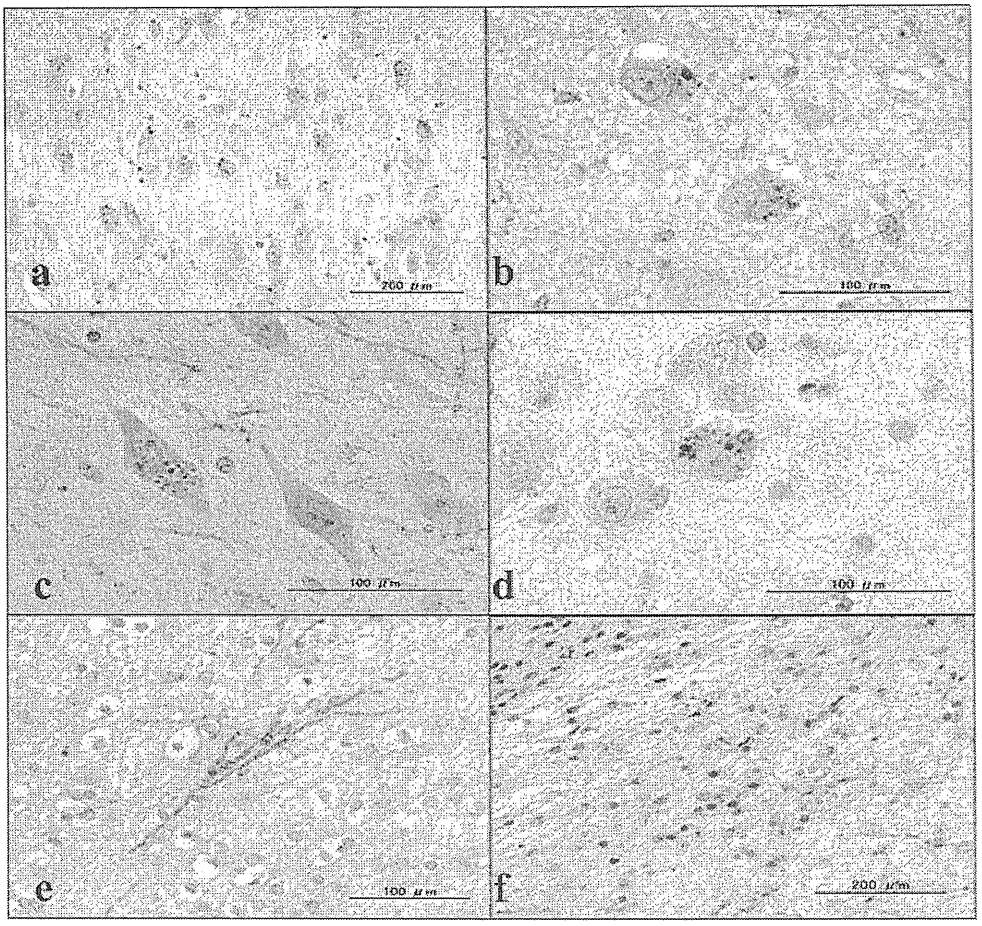

Fig. 5. pCREB immunoreactivity in AD and non-AD brains. The tissue sections of the hippocampus (HC) and the motor cortex (MC) of 11 AD patients and 13 other neurological disease (non-AD) patients were immunolabeled with an antibody against Ser-133-phosphorylated CREB (pCREB). (a) HC CA1 of a 59-year-old AD patient. The granular components of granulovacuolar degeneration (GVD) accumulated in the cytoplasm of pyramidal neurons exhibit strong pCREB immunoreactivity. (b) HC CA1 of a 68-year-old AD patient. The granular components of GVD accumulated in the cytoplasm of pyramidal neurons exhibit strong pCREB immunoreactivity. (c) HC CA3 of a 77 year-old AD patient. The vacuolar components of GVD are devoid of pCREB immunoreactivity. Neuritic processes of hippocampal neurons express variable levels of pCREB immunoreactivity. (d) HC CA1 of a 68 year-old myotonic dystrophy patient. The granular components of GVD accumulated in the cytoplasm of pyramidal neurons exhibit strong pCREB immunoreactivity. (e) MC of a 72-year-old AD patient. Substantial numbers of neuronal axons in the white matter of the motor cortex express strong pCREB immunoreactivity. (f) The periventricular white matter in the hippocampus of an 80 year-old AD patient. A subpopulation of reactive astrocytes express strong pCREB immunoreactivity located predominantly in their nuclei.

(JNK), c-Jun, pancreatic eIF2-alpha kinase (PERK), and TAR DNA-binding protein-43 (TDP-43), all of which are modified by phosphorylation, are found to be accumulated in GVD granules of hippocampal neurons in AD brains [38–43]. GVD granules also include cytoskeletal proteins, such as neurofilament, tubulin, and tau, along with ubiquitin [44,45]. At present, the precise implication of pCREB accumulation in GVD granules of hippocampal neurons in AD brains remains unknown. Importantly, degenerating neurons but not apparently healthy neurons in AD brains exhibit the profuse accumulation of autophagic vacuoles (AVs), owing to decreased clearance of AVs [46], suggesting an involvement of impaired autophagy function in formation of pCREB-accumulated GVD granules.

We found that neuronal axons, neuritic processes, and a subpopulation of reactive astrocytes also express pCREB immunoreactivity in both AD and non-AD brains. In a rat model of neuronal injury, reactive astrocytes express pCREB following intracerebroventricular injection of kinate [47]. In developing mouse DRG neurons, CREB protein is translated in response to NGF from the corresponding mRNA located in axons, and subsequently translocated to the cell body via a retro-

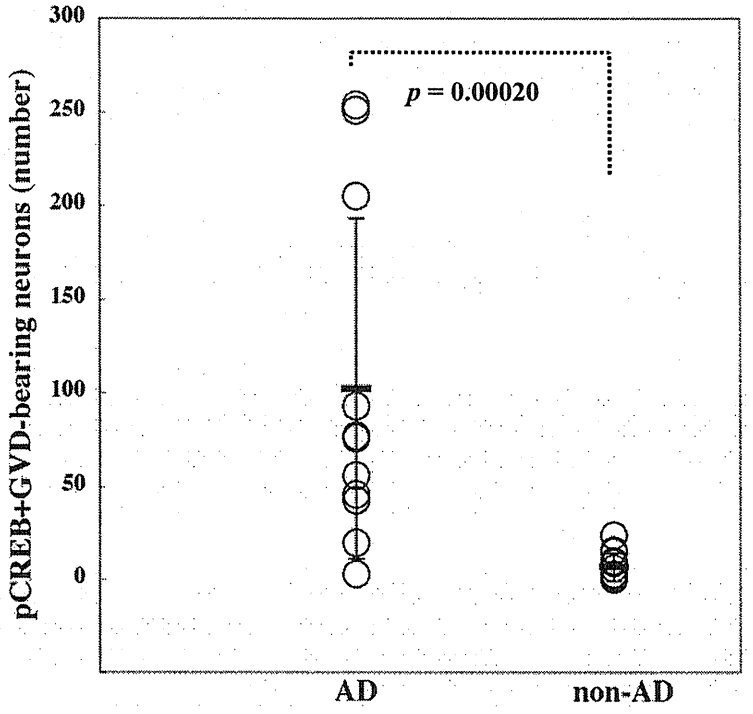

Fig. 6. The number of pCREB-immunoreactive GVD-bearing neurons in the hippocampus of AD and non-AD brains. The number of pCREB-immunoreactive GVD-bearing neurons was counted in the CA1, CA2, CA3 and CA4 sectors and the subiculum of the hippocampus, derived from 11 AD cases and 13 age and sex-matched other neurological disease (non-AD) cases. Non-AD cases include three patients with Parkinson disease (PD), two with multiple system atrophy (MSA), four with amyotrophic lateral sclerosis (ALS), and four with myotonic dystrophy. The total number in each case is plotted. The statistical difference in the numbers between AD and non-AD was evaluated by Mann-Whitney's U test.

grade axonal transport [48]. These observations would provide an explanation for glial or axonal location of CREB and pCREB.

We identified NF-κB-regulated gene expression as the second significant pathway in the molecular network of AGDs and IADGs (Supplementary Fig. 1 online). The NF-κB family, consisting of NF-κB1 (p50/p105), NF-κB2 (p52/p100), RelA (p65), RelB, and c-Rel, acts as a central regulator of innate and adaptive immune responses, cell proliferation, and apoptosis [49]. Under unstimulated conditions, NF-κB is sequestrated in the cytoplasm via non-covalent interaction with the inhibitor of NF-κB (IκB). Proinflammatory cytokines and stress-inducing agents activate specific IκB kinases that phosphorylate IκB proteins. Phosphorylated IκBs are ubiquitinated, and then processed for proteasome-mediated degradation, resulting in nuclear translocation of NF-κB that regulates the expression of hundreds of target genes by binding to the consensus sequence located in the promoter. Importantly, the expression of NF-κB p65 is enhanced in neurons, NFTs, and dystrophic neurites in the hippocampus and entorhinal cortex of AD brains [50]. A NF-κB-inducible microRNA, MiR-146a, reduces the expression of complement factor H (CFH), a negative regulator of proinflammatory responses in AD brains [51].

We also identified gene expression regulated by vitamin D receptor (VDR) as the third significant pathway in the molecular network of AGDs (Supplementary Fig. 2 online). Vitamin D plays a neuroprotective role by modulating neuronal calcium homeostasis. By forming a heterodimer with the retinoid X receptor (RXR), VDR activates the transcription of target genes with the vitamin D response element (VDRE) in the promoter. A significant association is found between VDR gene polymorphism and development of AD [52]. In AD brains, the expression of VDR and its target calbindin D28K is downregulated in hippocampal CA1 neurons [53].

In conclusion, KeyMolnet has effectively characterized molecular network of 2,883 ADGs and 559 IADGs. The common upstream search identified CREB as the principal transcription factor that regulates molecular networks of both ADGs and IADGs. Im-

munohistochemical study showed an abnormal accumulation of pCREB in GVD granules in hippocampal neurons of AD brains. These observations suggest that aberrant CREB-mediated gene regulation serves as a molecular biomarker of AD-related pathological processes, and support the hypothesis that sequestration of pCREB in GVD granules is in part responsible for deregulation of CREB-mediated gene expression in AD hippocampus.

5. Supplemental Material

Supplemental figures and tables can be found on http://www.my-pharm.ac.jp/~satoj/sub19.html as downloadable PDF files.

Acknowledegements

Human brain tissues were provided by Research Resource Network (RRN), Japan. This work was supported by a research grant to J-IS from the High-Tech Research Center Project, the Ministry of Education, Culture, Sports, Science and Technology (MEXT), Japan (S0801043), and from Research on Intractable Diseases, the Ministry of Health, Labour and Welfare of Japan.

References

[1] A. Serretti, P. Olgiati and D. De Ronchi, Genetics of Alzheimer's disease. A rapidly evolving field, *J Alzheimers Dis* **12** (2007), 73–92.

[2] S.F. Kingsmore, I.E. Lindquist, J. Mudge, D.D. Gessler and W.D. Beavis, Genome-wide association studies: progress and potential for drug discovery and development, *Nat Rev Drug Discov* **7** (2008), 221–230.

[3] S.D. Ginsberg, S.E. Hemby, V.M. Lee, J.H. Eberwine and J.Q. Trojanowski, Expression profile of transcripts in Alzheimer's disease tangle-bearing CA1 neurons, *Ann Neurol* **48** (2000), 77–87.

[4] V. Colangelo, J. Schurr, M.J. Ball, R.P. Pelaez, N.G. Bazan and W.J. Lukiw, Gene expression profiling of 12633 genes in Alzheimer hippocampal CA1: transcription and neurotrophic factor down-regulation and up-regulation of apoptotic and pro-inflammatory signaling, *J Neurosci Res* **70** (2002), 462–473.

[5] P. Katsel, C. Li and V. Haroutunian, Gene expression alterations in the sphingolipid metabolism pathways during progression of dementia and Alzheimer's disease: a shift toward ceramide accumulation at the earliest recognizable stages of Alzheimer's disease? *Neurochem Res* **32** (2007), 845–856.

[6] C. Williams, R. Mehrian Shai, Y. Wu, Y.H. Hsu, T. Sitzer, B. Spann, C. McCleary, Y. Mo and C.A. Miller, Transcriptome analysis of synaptoneurosomes identifies neuroplasticity genes overexpressed in incipient Alzheimer's disease, *PLoS ONE* **4** (2009), e4936.

[7] K. Oda, Y. Matsuoka, A. Funahashi and H. Kitano, A comprehensive pathway map of epidermal growth factor receptor signaling, *Mol Syst Biol* **1** (2005), 2005.0010.

[8] F. Noorbakhsh, C.M. Overall and C. Power, Deciphering complex mechanisms in neurodegenerative diseases: the advent of systems biology, *Trends Neurosci* **32** (2009), 88–100.

[9] R. Albert, H. Jeong and A.L. Barabasi, Error and attack tolerance of complex networks, *Nature* **406** (2000), 378–382.

[10] E.M. Blalock, J.W. Geddes, K.C. Chen, N.M. Porter, W.R. Markesbery and P.W. Landfield, Incipient Alzheimer's disease: microarray correlation analyses reveal major transcriptional and tumor suppressor responses, *Proc Natl Acad Sci USA* **101** (2004), 2173–2178.

[11] J.A. Miller, M.C. Oldham and D.H. Geschwind, A systems level analysis of transcriptional changes in Alzheimer's disease and normal aging, *J Neurosci* **28** (2008), 1410–1420.

[12] H. Sato, S. Ishida, K. Toda, R. Matsuda, Y. Hayashi, M. Shigetaka, M. Fukuda, Y. Wakamatsu and A. Itai, New approaches to mechanism analysis for drug discovery using DNA microarray data combined with KeyMolnet, *Curr Drug Discov Technol* **2** (2005) 89–98.

[13] D.W. Huang, B.T. Sherman and R.A. Lempicki, Systematic and integrative analysis of large gene lists using DAVID bioinformatics resources, *Nat Protoc* **4** (2009), 44–57.

[14] E.I. Boyle, S. Weng, J. Gollub, H. Jin, D. Botstein, J.M. Cherry and G. Sherlock, GO: TermFinder – open source software for accessing Gene Ontology information and finding significantly enriched Gene Ontology terms associated with a list of genes, *Bioinformatics* **20** (2004), 3710–3715.

[15] S.S. Mirra, A. Heyman, D. McKeel, S.M. Sumi, B.J. Crain, L.M. Brownlee, F.S. Vogel, J.P. Hughes, G. van Belle and L. Berg, The Consortium to Establish a Registry for Alzheimer's Disease (CERAD). Part II. Standardization of the neuropathologic assessment of Alzheimer's disease, *Neurology* **41** (1991), 479–486.

[16] H. Braak, I. Alafuzoff, T. Arzberger, H. Kretzschmar and K. Del Tredici, Staging of Alzheimer disease-associated neurofibrillary pathology using paraffin sections and immunocytochemistry, *Acta Neuropathol* **112** (2006), 389–404.

[17] T. Misawa, K. Arima, H. Mizusawa and J. Satoh, Close association of water channel AQP1 with amyloid-β deposition in Alzheimer disease brains, *Acta Neuropathol* **116** (2008), 247–260.

[18] B. Mayr and M. Montminy, Transcriptional regulation by the phosphorylation-dependent factor CREB, *Nat Rev Mol Cell Biol* **2** (2001), 599–609.

[19] B.E. Lonze and D.D. Ginty, Function and regulation of CREB family transcription factors in the nervous system, *Neuron* **35** (2002), 605–623.

[20] J. Satoh, Z. Illes, A. Peterfalvi, H. Tabunoki, C. Rozsa and T. Yamamura, Aberrant transcriptional regulatory network in T cells of multiple sclerosis, *Neurosci Lett* **422** (2007), 30–33.

[21] J. Satoh, T. Misawa, H. Tabunoki and T. Yamamura, Molecular network analysis of T-cell transcriptome suggests aberrant regulation of gene expression by NF-κB as a biomarker for relapse of multiple sclerosis, *Dis Markers* **25** (2008), 27–35.

[22] X. Zhang, D.T. Odom, S.H. Koo, M.D. Conkright, G. Canettieri, J. Best, H. Chen, R. Jenner, E. Herbolsheimer, E. Jacobsen, S. Kadam, J.R. Ecker, B. Emerson, J.B. Hogenesch, T. Unterman, R.A. Young and M. Montminy, Genome-wide analysis of cAMP-response element binding protein occupancy, phosphorylation, and target gene activation in human tissues, *Proc Natl Acad Sci USA* **102** (2005), 4459–4464.

[23] H. Viola, M. Furman, L.A. Izquierdo, M. Alonso, D.M. Barros, M.M. de Souza, I. Izquierdo and J.H. Medina, Phosphorylated cAMP response element-binding protein as a molecular marker of memory processing in rat hippocampus: effect of novelty, *J Neurosci* **20** (2000), RC112.

[24] M. Yamamoto-Sasaki, H. Ozawa, T. Saito, M. Rösler and P. Riederer, Impaired phosphorylation of cyclic AMP response element binding protein in the hippocampus of dementia of the Alzheimer type, *Brain Res* **824** (1999), 300–303.

[25] G.S. Griesbach, R.L. Sutton, D.A. Hovda, Z. Ying and F. Gomez-Pinilla, Controlled contusion injury alters molecular systems associated with cognitive performance, *J Neurosci Res* **87** (2009), 795–805.

[26] B. Gong, O.V. Vitolo, F. Trinchese, S. Liu, M. Shelanski and O. Arancio, Persistent improvement in synaptic and cognitive functions in an Alzheimer mouse model after rolipram treatment, *J Clin Invest* **114** (2004), 1624–1634.

[27] Z. Liang, F. Liu, I. Grundke-Iqbal, K. Iqbal and C.X. Gong, Down-regulation of cAMP-dependent protein kinase by over-activated calpain in Alzheimer disease brain, *J Neurochem* **103** (2007), 2462–2470.

[28] D.N. Arvanitis, A. Ducatenzeiler, J.N. Ou, E. Grodstein, S.D. Andrews, S.R. Tendulkar, A. Ribeiro-da-Silva, M. Szyf and A.C. Cuello, High intracellular concentrations of amyloid-β block nuclear translocation of phosphorylated CREB, *J Neurochem* **103** (2007), 216–228.

[29] O.V. Vitolo, A. Sant'Angelo, V. Costanzo, F. Battaglia, O. Arancio and M. Shelanski, Amyloid β-peptide inhibition of the PKA/CREB pathway and long-term potentiation: reversibility by drugs that enhance cAMP signaling, *Proc Natl Acad Sci USA* **99** (2002), 13217–13221.

[30] D. Puzzo, O. Vitolo, F. Trinchese, J.P. Jacob, A. Palmeri and O. Arancio, Amyloid-β peptide inhibits activation of the nitric oxide/cGMP/cAMP-responsive element-binding protein pathway during hippocampal synaptic plasticity, *J Neurosci* **25** (2005), 6887–6897.

[31] Q.L. Ma, M.E. Harris-White, O.J. Ubeda, M. Simmons, W. Beech, G.P. Lim, B. Teter, S.A. Frautschy and G.M. Cole, Evidence of Aβ- and transgene-dependent defects in ERK-CREB signaling in Alzheimer's models, *J Neurochem* **103** (2007), 1594–1607.

[32] Q. Li, H.F. Zhao, Z.F. Zhang, Z.G. Liu, X.R. Pei, J.B. Wang and Y. Li, Long-term green tea catechin administration prevents spatial learning and memory impairment in senescence-accelerated mouse prone-8 mice by decreasing $A\beta_{1-42}$ oligomers and upregulating synaptic plasticity-related proteins in the hippocampus, *Neuroscience* (2009), in press, doi:10.1016/j.neuroscience.2009.07.014.

[33] F.G. De Felice, A.P. Wasilewska-Sampaio, A.C. Barbosa, F.C. Gomes, W.L. Klein and S.T. Ferreira, Cyclic AMP enhancers and Aβ oligomerization blockers as potential therapeutic agents in Alzheimer's disease, *Curr Alzheimer Res* **4** (2007), 263–271.

[34] R.A. Nixon, Autophagy, amyloidogenesis and Alzheimer disease, *J Cell Sci* **120** (2007), 4081–4091.

[35] C.V. Garat, D. Fankell, P.F. Erickson, J.E. Reusch, N.N. Bauer, I.F. McMurtry and D.J. Klemm, Platelet-derived growth factor BB induces nuclear export and proteasomal degradation of CREB via phosphatidylinositol 3-kinase/Akt signaling in pulmonary artery smooth muscle cells, *Mol Cell Biol* **26** (2006), 4934–4948.

[36] S. Costes, B. Vandewalle, C. Tourrel-Cuzin, C. Broca, N. Linck, G. Bertrand, J. Kerr-Conte, B. Portha, F. Pattou, J. Bockaert and S. Dalle, Degradation of cAMP-responsive element-binding protein by the ubiquitin-proteasome pathway contributes to glucotoxicity in beta-cells and human pancreatic islets, *Diabetes* **58** (2009) 1105–1115.

[37] K. Okamoto, S. Hirai, T. Iizuka, T. Yanagisawa and M. Watanabe, Reexamination of granulovacuolar degeneration, *Acta Neuropathol* **82** (1991), 340–345.

[38] C. Stadelmann, T.L. Deckwerth, A. Srinivasan, C. Bancher, W. Brück, K. Jellinger and H. Lassmann, Activation of caspase-3 in single neurons and autophagic granules of granulovacuolar degeneration in Alzheimer's disease. Evidence for apoptotic cell death, *Am J Pathol* **155** (1999), 1459–1466.

[39] K. Leroy, A. Boutajangout, M. Authelet, J.R. Woodgett, B.H. Anderton and J.P. Brion, The active form of glycogen synthase kinase-3β is associated with granulovacuolar degeneration in neurons in Alzheimer's disease, *Acta Neuropathol* **103** (2002), 91–99.

[40] S. Lagalwar, R.W. Berry and L.I. Binder, Relation of hippocampal phospho-SAPK/JNK granules in Alzheimer's disease and tauopathies to granulovacuolar degeneration bodies, *Acta Neuropathol* **113** (2007), 63–73.

[41] A. Thakur, X. Wang, S.L. Siedlak, G. Perry, M.A. Smith and X. Zhu, c-Jun phosphorylation in Alzheimer disease, *J Neurosci Res* **85** (2007), 1668–1673.

[42] J.J. Hoozemans, E.S. van Haastert, D.A. Nijholt, A.J. Rozemuller, P. Eikelenboom and W. Scheper, The unfolded protein response is activated in pretangle neurons in Alzheimer's disease hippocampus, *Am J Pathol* **174** (2009), 1241–1251.

[43] A. Kadokura, T. Yamazaki, S. Kakuda, K. Makioka, C.A. Lemere, Y. Fujita, M. Takatama and K. Okamoto, Phosphorylation-dependent TDP-43 antibody detects intraneuronal dot-like structures showing morphological characters of granulovacuolar degeneration, *Neurosci Lett* (2009), in press, doi:10.1016/j.neulet.2009.06.024.

[44] D.W. Dickson, H. Ksiezak-Reding, P. Davies and S.H. Yen, A monoclonal antibody that recognizes a phosphorylated epitope in Alzheimer neurofibrillary tangles, neurofilaments and tau proteins immunostains granulovacuolar degeneration, *Acta Neuropathol* **73** (1987), 254–258.

[45] W. Bondareff, C.M. Wischik, M. Novak and M. Roth, Sequestration of tau by granulovacuolar degeneration in Alzheimer's disease, *Am J Pathol* **139** (1991), 641–647.

[46] B. Boland, A. Kumar, S. Lee, F.M. Platt, J. Wegiel, W.H. Yu and R.A. Nixon, Autophagy induction and autophagosome clearance in neurons: relationship to autophagic pathology in Alzheimer's disease, *J Neurosci* **28** (2008) 6926–6937.

[47] W.Y. Ong, H.M. Lim, T.M. Lim and B. Lutz, Kainate-induced neuronal injury leads to persistent phosphorylation of cAMP response element-binding protein in glial and endothelial cells in the hippocampus, *Exp Brain Res* **131** (2000), 178–186.

[48] L.J. Cox, U. Hengst, N.G. Gurskaya, K.A. Lukyanov and S.R. Jaffrey, Intra-axonal translation and retrograde trafficking of CREB promotes neuronal survival, *Nat Cell Biol* **10** (2008) 149–159.

[49] I Granic, A.M. Dolga, I.M. Nijholt, G. van Dijk and U.L. Eisel, Inflammation and NF-κB in Alzheimer's disease and diabetes, *J Alzheimers Dis* **16** (2009), 809–821.

[50] K. Terai, A. Matsuo and P.L. McGeer, Enhancement of immunoreactivity for NF-κB in the hippocampal formation and cerebral cortex of Alzheimer's disease, *Brain Res* **735** (1996), 159–168.

[51] W.J. Lukiw, Y. Zhao and J.G. Cui, An NF-κB-sensitive micro RNA-146a-mediated inflammatory circuit in Alzheimer

disease and in stressed human brain cells, *J Biol Chem* **283** (2008), 31315–31322.

[52] D. Gezen-Ak, E. Dursun, T. Ertan, H. Hanağasi, H. Gürvit, M. Emre, E. Eker, M. Oztürk, F. Engin and S. Yilmazer, Association between vitamin D receptor gene polymorphism and Alzheimer's disease, *Tohoku J Exp Med* **212** (2007), 275–282.

[53] M.K. Sutherland, M.J. Somerville, L.K. Yoong, C. Bergeron, M.R. Haussler and D.R. McLachlan, Reduction of vitamin D hormone receptor mRNA levels in Alzheimer as compared to Huntington hippocampus: correlation with calbindin-28k mRNA levels, *Brain Res Mol Brain Res* **13** (1992), 239–250.

Neuropathology and Applied Neurobiology (2009), **35**, 16–35 doi: 10.1111/j.1365-2990.2008.00947.x

Protein microarray analysis identifies human cellular prion protein interactors

J. Satoh*†, S. Obayashi*, T. Misawa*, K. Sumiyoshi*, K. Oosumi* and H. Tabunoki*

**Department of Bioinformatics and Molecular Neuropathology, Meiji Pharmaceutical University, and †Department of Immunology, National Institute of Neuroscience, NCNP, Tokyo, Japan*

J. Satoh, S. Obayashi, T. Misawa, K. Sumiyoshi, K. Oosumi and H. Tabunoki (2009) *Neuropathology and Applied Neurobiology* **35**, 16–35

Protein microarray analysis identifies human cellular prion protein interactors

Aims: To obtain an insight into the function of cellular prion protein (PrPC), we studied PrPC-interacting proteins (PrPIPs) by analysing a protein microarray. **Methods:** We identified 47 novel PrPIPs by probing an array of 5000 human proteins with recombinant human PrPC spanning amino acid residues 23–231 named PR209. **Results:** The great majority of 47 PrPIPs were annotated as proteins involved in the recognition of nucleic acids. Coimmunoprecipitation and cell imaging in a transient expression system validated the interaction of PR209 with neuronal PrPIPs, such as FAM64A, HOXA1, PLK3 and MPG. However, the interaction did not generate proteinase K-resistant proteins. KeyMolnet, a bioinformatics tool for analysing molecular interaction on the curated knowledge database, revealed that the complex molecular network of PrPC and PrPIPs has a significant relationship with AKT, JNK and MAPK signalling pathways. **Conclusions:** Protein microarray is a useful tool for systematic screening and comprehensive profiling of the human PrPC interactome. Because the network of PrPC and interactors involves signalling pathways essential for regulation of cell survival, differentiation, proliferation and apoptosis, these observations suggest a logical hypothesis that dysregulation of the PrPC interactome might induce extensive neurodegeneration in prion diseases.

Keywords: cellular prion protein, KeyMolnet, protein microarray, protein–protein interaction

Published online *Article Accepted* on 23th February 2008

Introduction

Prion diseases are a group of neurodegenerative disorders affecting both animals and humans [1,2]. The great majority of prion diseases are transmissible, and characterized by intracerebral accumulation of an abnormal prion protein (PrPSc) that is identical in amino acid sequence to the cellular isoform (PrPC) encoded by the *PRNP* gene. PrPC is expressed widely in neural and non-neural tissues at the highest level in neurones in the central nervous system (CNS) [3]. PrPSc differs biochemically from PrPC by its β sheet-enriched structure, detergent insolubility, limited proteolysis by proteinase K, a slower turnover rate and infectivity. Previous studies suggested that the protein conformational conversion of α-helix-rich PrPC into β sheet-rich PrPSc involves a homotypic interaction between endogenous PrPC and incoming or *de novo* generated PrPSc via a post-translational process mediated by as yet unidentified species-specific auxiliary factor(s) named 'protein X' [4,5].

At present, the biological function of PrPC remains largely unknown. Several lines of PrPC-deficient mice were established independently by different gene-targeting strategies [6–8]. All of them exhibited normal early development and complete protection against scrapie infection. These observations indicate that PrPC is dispensable for embryonic development, but is pivotal for inducing prion

Correspondence: Jun-ichi Satoh, Department of Bioinformatics and Molecular Neuropathology, Meiji Pharmaceutical University, 2-522-1 Noshio, Kiyose, Tokyo 204–8588, Japan. Tel: +81 42 4958678; Fax: +81 42 4958678; E-mail: satoj@my-pharm.ac.jp

diseases. Several *in vitro* studies suggested a role of PrPC in neuritogenesis [9,10], neuronal cell adhesion [11] and a receptor for neurotrophic factors [12]. More consistently, many studies indicated that an octapeptide repeat region of PrPC with a copper-binding capacity exhibits an antioxidant activity [13]. However, none of previous findings provided an adequate explanation for mild phenotypes of PrPC-deficient mice.

A number of previous studies, by employing mainly the yeast two-hybrid (Y2H) screening system, identified a wide variety of PrPC-interacting proteins (PrPIPs). They include synapsin I [14], glial fibrillary acidic protein [15], amyloid precursor-like protein 1 [16], heat shock protein Hsp60 [17–19], the Hsp cofactor STI-1 [20], the antiapoptotic molecule Bcl-2 [21], signal-transducing adapters such as Grb2 [14], ZAP70 [22] and 14-3-3 [23], neurotrophin receptor interacting MAGE homolog [24], tubulin [25], heterogeneous ribonuclear protein A2/B1 [26], casein kinase 2 [27], plasminogen [28], laminin receptor precursor [29], laminin [9] and vitronection [30]. Most of these molecules play a key role in signal-transducing events essential for neuronal function. However, none of them could serve as the chaperone 'protein X'.

The Y2H system is a powerful approach to identify novel protein–protein interactions. However, Y2H screening requires a lot of time and effort, and is often criticized for detecting the interactions unrelated to the physiological setting, and obtaining high rates of false positive interactors caused by spontaneous activation of reporter genes and self-activating bait proteins [31,32]. Recently, protein microarray technology has been established for rapid, systematic and less expensive screening of thousands of protein–protein interactions in a high-throughput fashion [33,34]. The array includes numerous protein targets of various functional classes immobilized on a single glass slide. The protein microarray has important applications in the areas not only of basic biological research on a whole-proteome scale, but also of drug discovery research of target identification [35,36].

In order to establish a therapeutic intervention targeted on prion propagation, it is essential to clarify the biological function of PrPC and the pathological implication of PrPSc, and equally important to identify all human PrPIPs, some of which potentially serve as a candidate for 'protein X'. The present study was designed to identify a comprehensive profile of the human PrPC interactome by analysing a high-density protein microarray, and to obtain an insight into the PrPC–PrPIPs network.

Materials and methods

Preparation of a V5-tagged PrP probe for microarray analysis

Human embryonic kidney cells HEK293, whose genome was modified for the Flp-In system (Flp-In 293; Invitrogen, Carlsbad, CA), contain a single Flp recombination target (FRT) site targeted for the site-specific recombination, integrated in a transcriptionally active locus of the genome, where it stably expresses the *lacZ*–Zeocin fusion gene driven from the pFRT/*lac*Zeo plasmid under the control of SV40 early promoter. The cells were maintained in Dulbecco's modified Eagle's medium supplemented with 10% foetal bovine serum, 100 U/ml penicillin and 100 μg/ml streptomycin (feeding medium) with inclusion of 100 μg/ml zeocin, as described previously [37].

To prepare the probe for protein microarray analysis, the gene encoding a truncated form of human PrPC spanning amino acid residues 23–231 named PR209 was amplified by polymerase chain reaction (PCR) using Pfu-Turbo DNA polymerase (Stratagene, La Jolla, CA) and the primer sets listed in Table S1 online. The PCR product was then cloned into a mammalian expression vector pSecTag/FRT/V5-His TOPO (Invitrogen) to produce a fusion protein with a C-terminal V5 tag, a C-terminal polyhistidine (6xHis) tag and an N-terminal Ig κ-chain secretion signal. This vector, together with the Flp recombinase expression vector pOG44 (Invitrogen), was transfected in Flp-In 293 cells by Lipofectamine 2000 reagent (Invitrogen). A stable cell line was established after incubating the transfected cells for 1 month in the feeding medium with inclusion of 100 μg/ml hygromycin B. In this system, the recombinant protein was secreted into the culture medium after the Ig κ-chain secretion signal sequence was processed by an endogenous signal peptidase-mediated cleavage.

To purify the V5-tagged PR209 protein, the serum-free culture supernatant was harvested, and concentrated at a 1/40 volume by centrifugation on an Amicon Ultra-15 filter (Millipore, Bedford, MA). It was then purified by the HIS-select spin column (Sigma, St. Louis, MO), and concentrated at a 1/10 volume by centrifugation on a Centricon-10 filter (Millipore). The protein concentration was determined by a Bradford assay kit (Bio-Rad, Hercules, CA). The purity and specificity of the probe were verified by Western blot analysis using mouse monoclonal anti-V5 antibody (Invitrogen), mouse monoclonal anti-

PrP antibody 3F4 (Dako, Tokyo, Japan) and rabbit polyclonal antibody C20 specific for the sequence close to the C-terminus of PrPC (Santa Cruz Biotechnology, Santa Cruz, CA). To determine the status of glycosylation, 5 μg of the probe protein was deglycosylated by incubating it at 37°C for 1.5 h with 5000 U peptide N-glycosidase F (New England BioLabs, Beverly, MA), followed by separation on the gel [37].

Protein microarray analysis

The present study utilized the ProtoArray human protein microarray v3.0 (Invitrogen). It contains approximately 5000 recombinant GST-tagged human proteins expressed by the baculovirus expression system and purified under native conditions by using gluthathione affinity chromatography to ensure the preservation of native structure, post-translational modifications and proper functionality of target proteins [36,38]. They were spotted in duplicate on a nitrocellulose-coated glass slide. The target proteins cover a wide range of biologically important proteins selected from the human ultimate open reading frame (ORF) clone collection (Invitrogen). The probe is spatially accessible to all parts of target proteins on the array, which protrude from the glass slide surface via the N-terminal GST fusion tag serving as a spacer. The complete list is shown in Table S2 online. The proteins are spotted in an arrangement of 4×12 subarrays equally spaced in vertical and horizontal directions. Each subarray includes 20×20 spots, composed of 76 positive and negative control spots (C), 222 human target proteins (H), and 102 blanks and empty spots (B) (Figure 1b). The 14 positive control spots include four of an Alexa Fluor 647-labelled antibody (row 1, columns 1, 2; row 14, columns 13, 14), six of a concentration gradient of a biotinylated anti-mouse antibody with a capacity to bind to mouse monoclonal anti-V5 antibody conjugated with Alexa Fluor 647 (row 14, columns 15–20), and four of a concentration gradient of V5 protein (row 15, columns 5–8). The 62 negative control spots include six of a concentration gradient of bovine serum albumin (BSA) (row 1, columns 3–8), four of a concentration gradient of a rabbit anti-GST antibody (row 1, columns 9–12), four of a concentration gradient of calmodulin (row 1, columns 13–16), 16 of a concentration gradient of GST (row 1, columns 17–20; row 2, columns 1–12), 10 of buffer only (row 15, columns 1, 2, 9–16), eight of human IgG subclasses (row 15, columns 17–20; row 16, columns 1–4), 12 of Invitrogen internal controls (row 4, columns 9, 10; row 6, columns 15–18; row 7, columns 9, 10, 15, 16; row 8, columns 13, 14), and two of an antibiotin antibody (row 15, columns 3, 4).

Non-specific binding was blocked by incubating the array for 90 min in the PBST blocking buffer composed of 1% BSA and 0.1% Tween 20 in phosphate-buffered saline (PBS). Then, it was incubated for 30 min at 4°C with the probe described above at a concentration of 200 μg/ml in the probing buffer composed of 1% BSA, 5 mM $MgCl_2$, 0.5 mM dithiothreitol, 0.05% Triton X-100 and 5% glycerol in PBS. The array was washed three times with the probing buffer, and then incubated for 30 min at 4°C with mouse monoclonal anti-V5 antibody labelled with Alexa Fluor 647 (Invitrogen) at a concentration of 260 ng/ml in the probing buffer. Then, the array was washed three times with the probing buffer, and scanned by the GenePix 4200 A scanner (Axon Instruments, Union City, CA) at a wavelength of 635 nm. The data were analysed by using the ProtoArray Prospector software v3.0 (Invitrogen), following acquisition of the microarray lot-specific information, which compensates inter-lot variations in protein concentrations identified by the post-printing quality control. According to the manufacturer-recommended setting of the ProtoArray Prospector software, the spots showing the background-subtracted signal intensity value greater than the median plus three standard deviations of all the fluorescence intensities were considered as having significant interactions. The Z-score, an indicator for statistical significance of binding specificity, was calculated as the background-subtracted signal intensity value of the target protein minus the average of the background-subtracted signal intensity value from the negative control distribution, divided by the standard deviation of the negative control distribution.

Bioinformatics analysis

The gene expression pattern of mouse orthologues of PrPIPs in the brain was searched on the Allen Brain Atlas database [39], an anatomically comprehensive digital atlas containing the expression patterns of more than 20 000 genes in the adult mouse brain analysed by high-throughput *in situ* hybridization methods (http://www.brain-map.org).

The interaction of PrPC with PrPIPs was searched on the Biomolecular Interaction Network database (BIND) (http://bond.unleashedinformatics.com). Functional

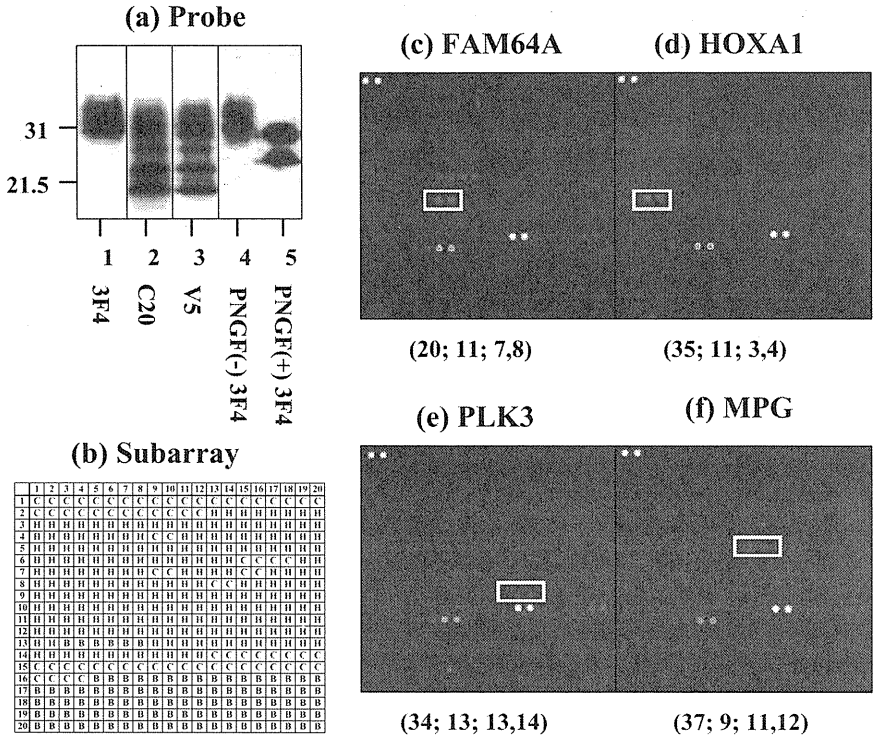

Figure 1. Protein microarray analysis. (a) Western blot of PR209 probe. The lanes (1–5) represent the immunolabelling with the antibodies following: (1) 3F4, (2) C20, (3) V5, (4) 3F4 before treatment with peptide N-glycosidase F (PNGase F) and (5) 3F4 after treatment with PNGase F. (b) The layout of subarray. The high-density protein microarray (5000 proteins, duplicate spots each) utilized in the present study contains 4 × 12 subarrays. Each subarray includes 20 × 20 spots. They are composed of 76 control spots (C) including 14 positive and 62 negative control spots, 222 human target proteins (H) and 102 blanks and empty spots (B), as described in *Materials and methods*. (c) FAM64A. The spot location is subarray 20, row 11, columns 7, 8. (d) HOXA1. Subarray 35, row 11, columns 3, 4. (e) PLK3. Subarray 34, row 13, columns 13, 14. (f) MPG. Subarray 37, row 9, columns 11, 12. PR209 interactors located on different subarrays (c–f) are indicated by an enclosed yellow line. It is worthy to note that in each subarray, positive control spots composed of an Alexa Fluor 647-labelled antibody (row 1, columns 1, 2; row 14, columns 13, 14), a concentration gradient of a biotinylated anti-mouse antibody with a capacity to bind to mouse monoclonal anti-V5 antibody conjugated with Alexa Fluor 647 (row 14, columns 15–20; signals visible on the higher concentration), and a concentration gradient of V5 protein (row 15, columns 5–8; signals visible on the higher concentration) are identified as positive, whereas negative control spots composed of a concentration gradient of BSA (row 1, columns 3–8), a concentration gradient of a rabbit anti-GST antibody (row 1, columns 9–12), a concentration gradient of calmodulin (row 1, columns 13–16), a concentration gradient of GST (row 1, columns 17–20; row 2, columns 1–12), buffer only (row 15; columns 1, 2, 9–16), human IgG subclasses (row 15, columns 17–20; row 16, columns 1–4), Invitrogen internal controls (row 4, columns 9, 10; row 6, columns 15–18; row 7, columns 9, 10, 15, 16; row 8, columns 13, 14), and an antibiotin antibody (row 15, columns 3, 4) are found as negative.

annotation of PrPIPs was searched by the web-accessible program named Database for Annotation, Visualization and Integrated Discovery (DAVID) version 2007, National Institute of Allergy and Infectious Diseases, National Institutes of Health (NIH) (http://david.abcc.ncifcrf.gov) [40]. It covers more than 40 annotation categories, including Gene Ontology terms, protein–protein interactions, protein functional domains, disease associations, biological pathways, sequence general features, homologies, gene functional summaries and tissue expressions. By importing the list of Entrez gene IDs of PrPIPs, this program creates the functional annotation chart, an annotation term-focused view that lists annotation terms and their associated genes under study. To avoid excessive counting of duplicated genes, the Fisher's exact statistics is calculated based on corresponding DAVID gene IDs by which all redundancies in original IDs are removed.

The molecular network of PrPIPs was analysed by the software named KeyMolnet (Institute of Medicinal Molecular Design, Tokyo, Japan) [41]. It operates on a comprehensive knowledge database, composed of information on relationships among human genes, molecules, diseases, pathways and drugs, carefully curated by expert biologists from review articles, literature and public

databases. They are categorized into the core contents collected from selected review articles with the highest reliability or the secondary contents extracted from abstracts of PubMed database and Human Reference Protein database.

By importing the list of Entrez gene IDs, KeyMolnet automatically provides corresponding molecules as a node on networks [41,42]. Among various network-searching algorithms, the 'N-points to N-points' search extracts the molecular network with the shortest route connecting the starting-point molecules and the end-point molecules. The generated network was compared side by side with 346 human canonical pathways of the KeyMolnet library. The algorithm counting the number of overlapping molecular relations between the extracted network and the canonical pathway makes it possible to identify the canonical pathway showing the most significant contribution to the extracted network. The significance in the similarity between both is scored following the formula, where O = the number of overlapping molecular relations between the extracted network and the canonical pathway, V = the number of molecular relations located in the extracted network, C = the number of molecular relations located in the canonical pathway, T = the number of total molecular relations (approximately 90 000 sets) and X = the sigma variable that defines incidental agreements.

$$\text{score} = -\log_2\left(\sum_{x=O}^{Min(C,V)} f(x)\right)$$

$$f(x) = {}_{C}C_{X} \cdot {}_{T-C}C_{V-x} / {}_{T}C_{V}$$

Immunoprecipitation and Western blot analysis

PR209, the N-terminal half of PR209 (amino acid residues 23–121), the C-terminal half of PR209 (amino acid residues 122–231), and the ORF of family with sequence similarity 64, member A (FAM64A), polo-like kinase 3 (PLK3), N-methylpurine-DNA glycosylase (MPG) and homeobox A1 (HOXA1) were amplified by PCR using PfuTurbo DNA polymerase and the primer sets listed in Table S1 online. They were then cloned into the mammalian expression vector p3XFLAG-CMV7.1 (Sigma) or pCMV-Myc (Clontech, Mountain View, CA) to express a fusion protein with an N-terminal Flag or Myc tag. At 48 h after co-transfection of the vectors, HEK293 cells were homogenized in M-PER lysis buffer (Pierce, Rockford, IL) supplemented with a cocktail of protease inhibitors (Sigma). In limited experiments, a proteasome inhibitor MG-132 (Merck-Calbiochem, Tokyo, Japan) was added at a final concentration of 10 μM in the culture medium during the last 24 h before harvest. After preclearance, the supernatant was incubated at 4°C for 3 h with mouse monoclonal anti-Flag M2 affinity gel (Sigma), rabbit polyclonal anti-Myc-conjugated agarose (Sigma) or the same amount of normal mouse or rabbit IgG-conjugated agarose (Santa Cruz Biotechnology). After several washes, the immunoprecipitates were processed for Western blot analysis using rabbit polyclonal anti-Myc antibody (Sigma) and mouse monoclonal anti-FLAG M2 antibody (Sigma). The specific reaction was visualized using a chemiluminescence substrate (Pierce).

To determine the proteinase K-resistant property of PR209, the cells were homogenized in M-PER lysis buffer without inclusion of protease inhibitors. The protein extract was then incubated at 37°C for 30 min with 5 μg/ml recombinant proteinase K (Roche Diagnostics, Mannheim, Germany), followed by adding phenylmethylsulphonyl fluoride at a final concentration of 5 mM, according to the methods described previously [43]. Proteins were precipitated by adding 6% trichloroacetic acid. After centrifugation at 4°C for 15 min at 16 100 g, the pellets were washed with cold acetone, and processed for Western blot analysis using 3F4 antibody.

To determine the detergent-insoluble property of PR209, the cells were homogenized in a lysis buffer containing 100 mM NaCl, 10 mM EDTA, 10 mM Tis (pH 7.4), 0.5% Nonidet P-40 and 0.5% sodium deoxycholate, according to the methods described previously [44]. The lysate was centrifuged at 4°C for 10 min at 2000 g to remove debris. Then, the supernatant was further centrifuged at 4°C for 1 h at 16 100 g to separate detergent-soluble (supernatant) and detergent-insoluble (pellet) fractions. They were processed for Western blot analysis using 3F4 antibody. HRP-conjugated secondary antibodies were obtained from Santa Cruz Biotechnology.

Cell imaging analysis

PR209 and the ORF of FAM64A, PLK3, MPG and HOXA1 were amplified by PCR using PfuTurbo DNA polymerase and the primer sets listed in Table S1 online. They were then cloned into the mammalian expression vector pDsRed-Express-C1 (Clontech), pEYFP-C1 (Clontech), pcDNA3.1/NT/GFP-TOPO (Invitrogen) or pcDNA3.1/CT/GFP-TOPO (Invitrogen) to express a fusion protein with an N-terminal or C-terminal DsRed, EYFP or GFP tag. At 24–48 h after co-transfection of the vectors, the cells were

fixed briefly in 4% paraformaldehyde, mounted on slides with glycerol-polyvinyl alcohol, and examined on the Olympus BX51 universal microscope.

Human neural cell lines and cultures

Human astrocytes (AS) in culture were established from neuronal progenitor (NP) cells of human foetal brain (Cambrex, Walkersville, MD). For the induction of neuronal differentiation, NTera2 cells maintained in the undifferentiated state (NTera2-U) were incubated for 4 weeks in feeding medium containing 10^{-5} M *all trans* retinoic acid (Sigma), replated twice and then plated on a surface coated with Matrigel Basement Membrane Matrix (Becton Dickinson, Bedford, MA). They were incubated for another 2 weeks in feeding medium containing a cocktail of mitotic inhibitors, resulting in the enrichment of differentiated neurones (NTera2-N), as described previously [45]. Human microglia cell line HMO6 was provided by Dr Seung U. Kim, Division of Neurology, University of British Columbia, Vancouver, B.C., Canada. Total RNA of the human frontal cerebral cortex was obtained from Clontech.

Reverse transcription-PCR analysis

DNase-treated total cellular RNA was processed for cDNA synthesis using oligo$(dT)_{12-18}$ primers and SuperScript II reverse transcriptase (Invitrogen). Then, cDNA was amplified by PCR using HotStar Taq DNA polymerase (Qiagen, Valencia, CA) and a panel of primer sets listed in Table S1 online. The amplification program consisted of an initial denaturing step at 95°C for 15 min, followed by a denaturing step at 94°C for 1 min, an annealing step at 60°C for 40 s and an extension step at 72.9°C for 50 s for 30–35 cycles, except for the glyceraldehyde-3-phosphate dehydrogenase (G3PDH), an internal control, amplified for 27 cycles.

Results

Protein microarray analysis identified 47 novel PrPC interactors

To analyse the human protein microarray, V5-tagged PR209 probe was purified from the supernatant of a stable cell line secreting the recombinant protein in the culture medium. By Western blot analysis, the probe was composed of a mixture of glycosylated full-length and N-terminally truncated forms of PrPC (Figure 1**a**, lanes 1–5). The 18.5-kDa protein identified by C20 but not by 3F4 represents the C-terminal fragment produced by constitutive metalloprotease-mediated cleavage [46]. Among total 5000 proteins on the array, 47 were identified as the proteins showing significant interaction with the probe (Table 1). They include FAM64A (Figure 1**c**), HOXA1 (Figure 1**d**), casein kappa (CSN3), bromodomain adjacent to zinc finger domain, 2B (BAZ2B), chromosome 7 ORF 50 (C7orf50), surfeit 2 (SURF2), sodium channel modifier 1 (SCNM1), chromosome 18 ORF 56 (C18orf56), PLK3 (Figure 1**e**), RNA binding motif protein 22 (RBM22), hypothetical protein DKFZp761B107, MPG (Figure 1**f**), zinc finger protein 192 (ZNF192), thymic stromal lymphopoietin (TSLP), DEAD box polypeptide 47 (DDX47), MAP/microtubule affinity-regulating kinase 4 (MARK4), zinc finger protein 408 (ZNF408), TBP-like 1 (TBPL1), activator of basal transcription 1 (ABT1), ribosomal protein L41 (RPL41), zinc finger protein 740 (ZNF740), CWC15 homolog, four and a half LIM domains 1 (FHL1), amyotrophic lateral sclerosis 2 chromosome region, candidate 4 (ALS2CR4), immediate early response 3 (IER3), KIAA1191, peptidyl-tRNA hydrolase 1 homolog (PTRH1), phosphodiesterase 4D interacting protein (PDE4DIP), Rho GTPase activating protein 15 (ARHGAP15), mitochondrial GTPase 1 homolog (MTG1), cirrhosis, autosomal recessive 1 A (CIRH1A), eukaryotic translation initiation factor 2C, 1 (EIF2C1), WD repeat domain 5 (WDR5), centaurin, alpha 2 (CENTA2), protein phosphatase 1, regulatory subunit 14 A (PP1R14 A), cold inducible RNA binding protein (CIRBP), zinc finger, FYVE domain containing 28 (ZFYVE28), within bgcn homolog (WIBG), nucleolar protein family A, member 2 (NOLA2), PTPRF interacting protein, binding protein 2 (PPFIBP2), family with sequence similarity 27, member E3 (FAM27E3), fibroblast growth factor 13 (FGF13), apoptosis-inducing factor, mitochondrion-associated, 3 (AIFM3), 2′,3′-cyclic nucleotide 3′ phosphodiesterase (CNP), NIN1/RPN12 binding protein 1 homolog (NOB1), RNA-binding region containing 3 (RNPC3) and dual-specificity tyrosine-phosphorylation regulated kinase 3 (DYRK3). The gene expression pattern of PrPC interactors (PrPIPs) in the adult brain analysed by *in situ* hybridization was searched on the Allen Brain Atlas database [39]. Among 47 PrPIPs, at least 35 mouse orthologues (74%) were expressed in various regions of the adult mouse brain (Table 1). The expression pattern of the remaining

